

Raman Study of Synthetic Witherite–Strontianite Solid Solutions

Nuria Sánchez-Pastor^{1,2},
Alexander M. Gigler^{2,3},
Guntram Jordan²,
Wolfgang W. Schmahl²,
and Lurdes Fernández-Díaz^{1,4}

¹Departamento de Cristalografía y Mineralogía, Facultad de Ciencias Geológicas, Universidad Complutense de Madrid (UCM), Madrid, Spain

²Department für Geo- und Umweltwissenschaften, Ludwig-Maximilians-Universität (LMU), Munich, Germany

³Center for NanoScience (CeNS), Ludwig-Maximilians-Universität (LMU), Munich, Germany

⁴Instituto de Geociencias (UCM-CSIC), Madrid, Spain

ABSTRACT Characterization of zoned crystals of a synthetic witherite–strontianite solid solution ($\text{Ba}_x\text{Sr}_{1-x}\text{CO}_3$) was carried out using electron microprobe analysis and Raman spectroscopy. The sample was obtained by coprecipitation using the silica gel method. As each carbonate crystal from this preparation showed the whole range of intermediate compositions $\text{Ba}_x\text{Sr}_{1-x}\text{CO}_3$, $0.1 \leq x \leq 0.9$, the solid solution could be studied for single crystals. Peak-shape analysis of the Raman bands showed that the peak shifts depend on the replacement of the Ba and Sr cations introducing different radii and masses. We observed a shift to higher wave numbers for an increase of the SrCO_3 content.

KEYWORDS carbonates, Raman spectroscopy, replacement, solid solution, witherite–strontianite

INTRODUCTION

Despite the important geochemical implications of the Sr/Ba ratio of natural $\text{Ba}_x\text{Sr}_{1-x}\text{CO}_3$ crystals, the witherite (BaCO_3)–strontianite (SrCO_3) solid solution series remained subject to controversy. The fact that intermediate compositions of $\text{Ba}_x\text{Sr}_{1-x}\text{CO}_3$ are scarce in nature supported the idea of the existence of a miscibility gap at low temperatures.^[1] However, intermediate compositions were easily obtained synthetically, and experimental thermodynamic studies confirmed the ideality of this solid solution.^[2] Previous work also showed that $\text{Ba}_x\text{Sr}_{1-x}\text{CO}_3$ crystals always grew homogeneously because, due to the similarity of the solubility products of the end-members witherite and strontianite, the substituting ions Ba^{2+} and Sr^{2+} incorporate in the solid in the same stoichiometric proportion as in the aqueous phase.^[3] In contrast, $\text{Ba}_x\text{Sr}_{1-x}\text{SO}_4$ crystals grown in gels were always zoned because the large difference between the solubility products of the end members barite (BaSO_4) and celestite (SrSO_4) determine a strong ion partitioning between the solid solution and the aqueous solution.^[3,4] Zoned Ba–Sr carbonate crystals could be obtained in gel experiments using mixed $\text{SO}_4^{2-}/\text{CO}_3^{2-}$ solutions as anionic reactant. In these mixed solutions,

zoned $\text{Ba}_x\text{Sr}_{1-x}\text{SO}_4$ crystals were initially formed that subsequently were replaced by $\text{Ba}_x\text{Sr}_{1-x}\text{CO}_3$ pseudomorphically.^[5–7] The secondary $\text{Ba}_x\text{Sr}_{1-x}\text{CO}_3$ crystals inherited the complete range of intermediate compositions from the

precursor $\text{Ba}_x\text{Sr}_{1-x}\text{SO}_4$ crystals. Thus, carbonate-sulphate replacement is a highly valuable synthesis tool for solid solutions.

Only few authors have reported spectroscopic data on the witherite–strontianite solid solution.^[8,9] Homogenous $\text{Ba}_x\text{Sr}_{1-x}\text{CO}_3$ crystals grown in counter-diffusion experiments with porous silica gel at room temperature were characterized using Fourier transform infrared spectroscopy.^[9]

OBJECTIVE

This work focused on the applicability of combining micro-Raman spectroscopy and electron microprobe analysis in the research of mineral zoning.^[10] A major aim was to study the dependence of the Raman spectral characteristics on the composition of this solid solution. The large variety of intermediate compositions present in individual gel grown crystals made them especially useful for obtaining a comprehensive Raman data set of the witherite–strontianite solid solution.

MATERIALS AND METHODS

Gel Experiments

The experimental setup consisted of a U tube where silica hydrogel was placed in the horizontal branch, and the growth solutions ($0.9\text{ M BaCl}_2 + 0.1\text{ M SrCl}_2$ and $0.5\text{ M Na}_2\text{CO}_3 + 0.3\text{ M Na}_2\text{SO}_4$ ^[11]) were contained in the two vertical branches (Fig. 1). One month after we started counterdiffusion, crystals formed within the gel. The crystals were recovered from the gel 1 year after nucleation.

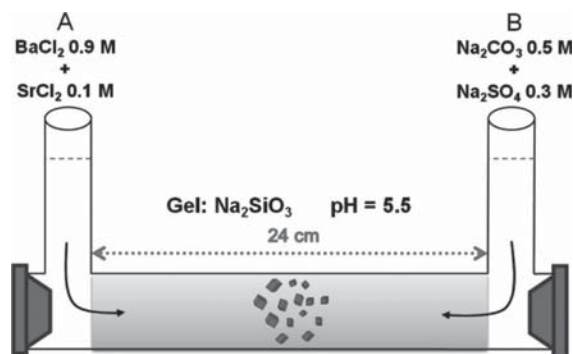


FIGURE 1 Experimental setup used for crystal growth.

Characterization of the Solid Solution

Crystals with morphologies representative for barite were hand-picked and studied using scanning electron microscopy (JEOL JSM6400, 40 kV) equipped with a LINK Ex1 energy dispersive spectrometer. In order to study the compositional zonation patterns, the crystals were mounted on glass slides, embedded in epoxy resin, polished, carbon coated, and studied by back-scattered electron (BSE) imaging. Variations in composition lead to contrasts^[12] that allow the researcher to distinguish Ba-rich and Sr-rich regions. Analysis revealed that the crystals were $\text{Ba}_x\text{Sr}_{1-x}\text{CO}_3$ pseudomorphs after $\text{Ba}_x\text{Sr}_{1-x}\text{SO}_4$. Some of the crystals were further characterized by electron microprobe analysis (JEOL Superprobe JXA-8900 M).

Raman spectra were obtained using a confocal Raman microscope (WITec alpha 300 R) equipped with a SHG Nd:YAG laser (532 nm, maximal power = 22.5 mW) and a lens-based spectrometer. Elastically scattered photons were rejected by a long pass filter, that is, only the Stokes shifts were recorded. Using a 600 mm^{-1} diffraction grating, the nominal spectral resolution was 3.5 cm^{-1} per CCD pixel. Spectra were recorded at 5 mW laser power with an integration time of 1 and 5 s with 10-fold averaging close to the spots where the microprobe analyses were conducted. A $100\times$ microscope objective (working distance = 0.26 mm, NA 0.90) was used for the measurements.

RESULTS

The $\text{Ba}_x\text{Sr}_{1-x}\text{CO}_3$ crystals as well as the end members BaCO_3 and SrCO_3 were recovered from the gel after 1 year. The $\text{Ba}_x\text{Sr}_{1-x}\text{CO}_3$ crystals showed progressive and oscillatory zonings. Figure 2a shows a crystal used for both electron microprobe and Raman analysis. The crystal was chosen because it contained all intermediate compositions of the strontianite–witherite solid solution from a Ba molar fraction x of 0.1–0.9. The quantitative analyses obtained by electron microprobe analysis (Fig. 2b) show an oscillatory zoning between the endpoints 1 and 2.

Raman spectra were recorded within $15\text{--}20\text{ }\mu\text{m}$ from the positions of the microprobe analyses in order to avoid locations possibly altered by EMPA

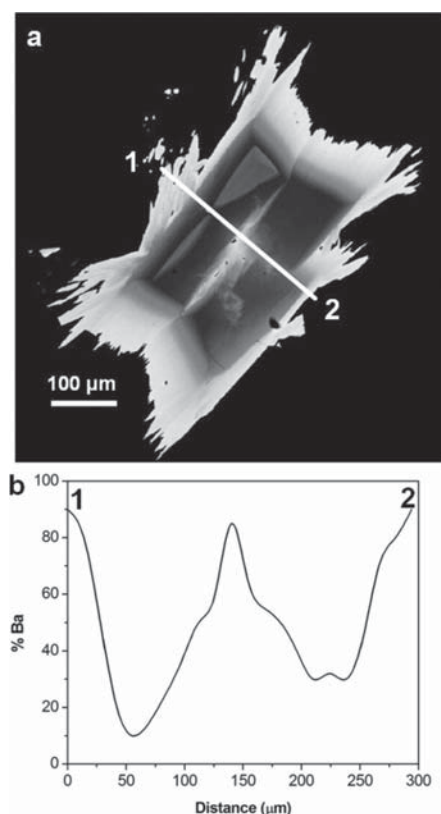


FIGURE 2 (a) BSE image of a polished $\text{Ba}_x\text{Sr}_{1-x}\text{CO}_3$ crystal showing the progressive and oscillatory zoning. (b) Composition profile along the line from point 1 to point 2 shown in image a.

measurements. The Raman modes of carbonates with aragonite structure are classified into two types: (i) internal vibration modes of CO_3^{2-} groups and (ii) external lattice modes involving vibrations of the divalent cations versus librations and displacements of the CO_3^{2-} groups.^[13] Within our accessible spectral range, 6 bands out of the 30 predicted Raman-active modes can be observed.^[14,15] The intense band corresponds to the ν_1 symmetric stretching mode of carbonate group. The Raman bands attributed to the ν_3 asymmetric stretching mode and the ν_4 asymmetric bending mode were also observed. The appearance of two lines corresponding to ν_3 is in accordance with the splitting of ν_3 predicted by theory. The ν_2 internal mode is not Raman active. The characteristic Raman bands due to the external vibration mode between 100 and 300 cm^{-1} are also present. Table 1 compiles the wave numbers of the vibration modes observed for our sample. Note that the Raman spectra of the end members of the solid solution were acquired on gel-grown crystals of pure strontianite and pure witherite. The wave numbers obtained

TABLE 1 Raman Data of the Witherite–Strontianite Solid Solution Obtained from the Crystal Shown in Fig. 2a

X_{Ba}	Lattice modes (cm^{-1})	ν_1 (cm^{-1})	ν_3 (cm^{-1})	ν_4 (cm^{-1})
0*	149, 183, 249	1073	1446, 1546	701
0.1	148, 179, 246	1071	1440, 1540	698
0.2	146, 174, 244	1070	1438, 1537	698
0.3	145, 172, 242	1068	1436, 1533	697
0.4	143, 171, 240	1067	1435, 1530	696
0.5	143, 168, 239	1066	1433, 1530	696
0.6	142, 165, 237	1065	1430, 1520	695
0.7	141, 162, 235	1063	1427, 1516	695
0.8	140, 160, 233	1061	1425, 1515	693
0.9	139, 155, 228	1060	1422, 1511	693
1*	136, 153, 226	1059	1422, 1511	692

*Data recorded on gel grown crystals of pure strontianite and pure witherite.

for the end members agree well with previous reports.^[4,5,16]

The variation of wave numbers of internal and lattice modes was studied as a function of the chemical composition. Figure 3a shows a comparison of the ν_1 fundamental in the Raman spectra of the intermediate compositions with 0.8, 0.4, and 0.1 Ba molar fraction of the witherite–strontianite solid solution. Obviously, this mode appears as a single band, and its wave numbers change linearly with the mole fraction of Ba.

Figure 3b shows the ν_3 fundamental. In trigonal symmetry, the ν_3 mode is doubly degenerate, and it splits into a doublet due to the orthorhombic symmetry of the crystalline field.^[13] The double band appears at 1446 cm^{-1} and 1546 cm^{-1} for pure strontianite and at 1422 cm^{-1} and 1511 cm^{-1} for pure witherite. As in the case of the ν_1 mode, there is a shift towards higher wave numbers with increasing Sr contents. Finally, Fig. 3c and Fig. 3d show the bands corresponding to the antisymmetric bending (ν_4) and the lattice modes, respectively. Both plots represent the same characteristics as the plots explained above with a shift towards higher wave numbers with increasing Sr content.

DISCUSSION

The combined EMPA and confocal-Raman analyses indicate that the zoned crystal covers a complete $\text{Ba}_x\text{Sr}_{1-x}\text{CO}_3$ solid solution between $x=0.9$ and $x=0.1$ without any two-phase gap. All spectra of the end members and the intermediate compositions

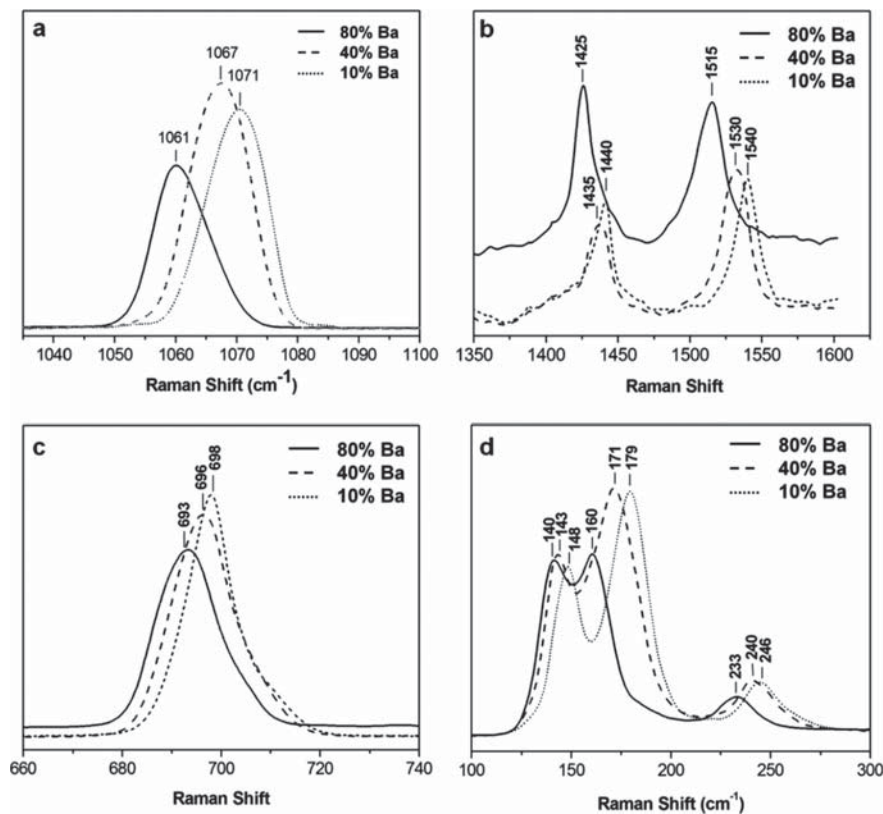


FIGURE 3 (a) Carbonate anion symmetric stretching bands (ν_1). (b) Carbonate anion asymmetric stretching bands (ν_3). (c) Carbonate anion asymmetric bending bands (ν_4). (d) Lattice modes.

of the witherite–strontianite solid solution show the fundamental internal modes and the lattice modes. The peak positions of the Raman-spectra are displayed in Fig. 4a. The ν_1 , ν_3 , and ν_4 internal modes arise from the symmetric stretching, the asymmetric stretching, and the in-plane bending mode of the carbonate ion group, respectively. For all modes, the progressive increase of the vibrational frequencies with increasing Sr/Ba ratio is linear, and regression

analysis shows correlation coefficients very close to unity as shown in Fig. 4b). Similar band shifts were observed by Chen et al.,^[17] who studied the Raman spectra of the end members and the intermediate compositions of the barite–celestite solid solution. In both solid solutions, such band shifts are a consequence of the decreasing effective mass of the oscillators and the increasing force constant with increasing Sr content. The radius of Ba^{2+} is larger

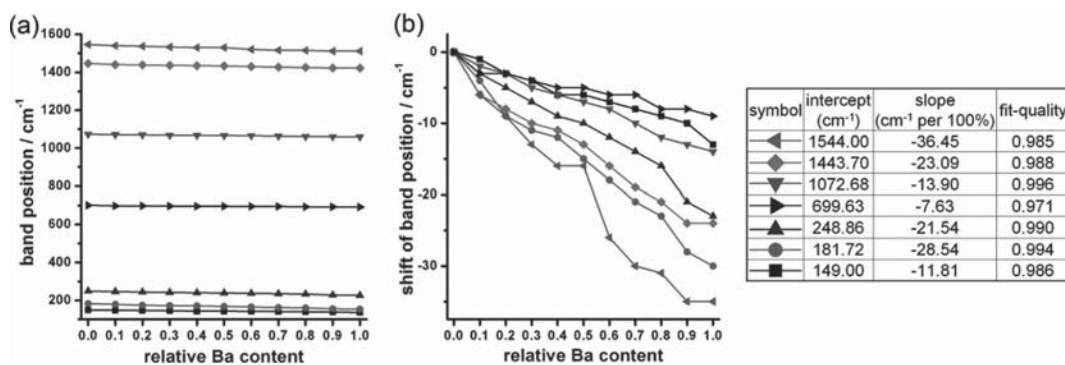


FIGURE 4 (a) Raman band positions depending on the composition of the solid solution. (b) relative shift of the band positions shown in image a together with the linear regression results.

(1.6 Å) than that of Sr^{2+} (1.44 Å). As a result, the Sr-O bond-length is shorter, and its bonding strength is higher than that of Ba-O.

ACKNOWLEDGMENTS

Nuria Sánchez-Pastor gratefully acknowledges the fellowship from the Humboldt Foundation. Financial support has been provided by project CGL2010-20134-C02-01 (Spanish Ministry of Science and Innovation). We thank the Microscopy Centre of the Complutense University for technical assistance and support. We are also grateful to Robert W. Stark (TU Darmstadt) for enabling Raman measurements.

REFERENCES

- Baldasari, A.; Speer, J. A. Witherite composition, physical properties, and genesis. *American Mineralogist* **1979**, *64*, 742–747.
- Chang, L. L. Y. Subsolidus phase relations in aragonite-type carbonates: 1. System $\text{CaCO}_3\text{-SrCO}_3\text{-BaCO}_3$. *American Mineralogist* **1971**, *56*, 1660–1673.
- Prieto, M.; Fernández-González, A.; Putnis, A.; Fernández-Díaz, L. Nucleation, growth, and zoning phenomena in crystallizing $(\text{Ba,Sr})\text{CO}_3$, $\text{Ba}(\text{SO}_4, \text{CrO}_4)$, $(\text{Ba,Sr})\text{SO}_4$, and $(\text{Cd,Ca})\text{CO}_3$ solid solutions from aqueous solutions. *Geochimica et Cosmochimica Acta* **1997**, *61*, 3383–3397.
- Sánchez-Pastor, N.; Pina, C. M.; Fernandez-Diaz, L. Relationships between crystal morphology and composition in the $(\text{Ba,Sr})\text{SO}_4\text{-H}_2\text{O}$ solid solution-aqueous solution system. *Chemical Geology* **2006**, *25*, 266–277.
- Sánchez-Pastor, N.; Pina, C. M.; Fernandez-Diaz, L. A combined in situ AFM and SEM study of the interaction between celestite (001) surfaces and carbonate-bearing aqueous solutions. *Surface Science* **2007**, *601*, 2973–2982.
- Sánchez-Pastor, N.; Pina, C. M.; Fernandez-Diaz, L. The effect of CO_3^{2-} on the growth of barite {001} and {210} surfaces: An AFM study. *Surface Science* **2006**, *600*, 1369–1381.
- Prieto, M.; Putnis, A.; Fernández-Díaz, L. Crystallization of solid-solutions from aqueous-solutions in a porous-medium: Zoning in $(\text{Ba,Sr})\text{SO}_4$. *Geological magazine* **1993**, *130*, 289–299.
- White, W. B. The carbonate minerals. In Farmer, V. C. (Ed.), *The Infrared Spectra of Minerals*; Mineralogical Society Monograph **1974**, 227–315.
- Böttcher, M. E.; Gehlken, P. L.; Fernández-González, A.; Prieto, M. Characterization of synthetic $\text{BaCO}_3\text{-SrCO}_3$ (witherrite-strontianite) solid solutions by Fourier transform infrared spectroscopy. *European Journal of Mineralogy* **1997**, *9*, 519–528.
- Sánchez-Pastor, N.; Gigler, A. M.; Cruz, J. A.; Park, S.-H.; Jordan, G. Fernández-Díaz, L. Growth of calcium carbonate in the presence of Cr(VI). *Crystal Growth and Design* **2011**, *11*(7), 3081–3089.
- Henisch, H. K.; García-Ruiz, J. M. Crystal growth in gels and Liesegang ring formation: I. Diffusion relationships. *Journal of Crystal Growth* **1986**, *75*, 195–202.
- Lloyd, G. E. Atomic number and crystallographic contrast images with the SEM: A review of black-scattered electron techniques. *Mineralogical Magazine* **1987**, *51*, 3–19.
- Alía, J. M.; Díaz de Mera, Y. D.; Edwards, H. G. M.; Martín, P. G.; Andrés, S. L. FT-Raman and infrared spectroscopic study of aragonite-strontianite $(\text{Ca}_x\text{Sr}_{1-x}\text{CO}_3)$ solid solution. *Spectrochimica Acta Part A-Molecular and Biomolecular Spectroscopy* **1997**, *53*, 2347–2362.
- Krishnamurti, D. The Raman spectra of aragonite, strontianite and witherrite. *Proceedings of the Indian Academy Sciences, Section A* **1960**, *51*(6), 285–295.
- Urmos, J.; Sharma, S. K.; Mackenzie, F. T. Characterization of some biogenic carbonates with Raman spectroscopy. *American Mineralogist* **1991**, *76*, 641–646.
- Coleyshaw, E. E.; Griffith, W. P.; Bowell, R. J. Fourier transform-Raman spectroscopy of minerals. *Spectrochimica Acta Part A* **1994**, *50*, 1909–1918.
- Chen, Y.-H.; Huang, E.; Yu, S.-C. High pressure Raman study on the $\text{BaSO}_4\text{-SrSO}_4$ series. *Solid State Communications* **2009**, *149*, 2050–2052.

Copyright of Spectroscopy Letters is the property of Taylor & Francis Ltd and its content may not be copied or emailed to multiple sites or posted to a listserv without the copyright holder's express written permission. However, users may print, download, or email articles for individual use.